CORROSION SCIENCE AND TECHNOLOGY, Vol.2, No.2(2003), pp.68~74

Effect of Niobium on the Electronic Properties of Passive Films on Zirconium Alloys

Bo Young Kim and Hyuk Sang Kwon

Dept. of Materials Science and Engineering, Korea Advanced Institute of Science and Technology
373-1, KuSongDong, YuSongGu, TaeJon, Korea, 305-701

The effects of Niobium on the structure and properties(especially electric properties) of passive film of Zirconium alloys in pH 8.5 buffer solution are examined by the photo-electrochemical analysis. For Zr-xNb alloys (x = 0, 0.45, 1.5, 2.5 wt%), photocurrent began to increase at the incident energy of 3.5 ~ 3.7 eV and exhibited the 1st peak at 4.3 eV and the 2nd peak at 5.7 eV. From $(i_{ph}\ h\nu)^{1/2}$ vs. $h\nu$ plot, indirect band gap energies E_g^1 = 3.01~3.47 eV , E_g^2 = 4.44~4.91 eV were obtained. With increasing Nb content, the relative photocurrent intensity of 1st peak significantly increased. Compared with photocurrent spectrum of thermal oxide of Zr-2.5Nb, It was revealed that 1st peak in photocurrent spectrum for the passive film formed on Zr-Nb alloy was generated by two types of electron transitions; the one caused by hydrous ZrO_2 and the other created by Nb. Two electron transition sources were overlapped over the same range of incident photon energy. In the photocurrent spectrum for passive film formed on Zr-2.5Nb alloy in which Nb is dissolved into matrix by quenching, the relative photocurrent intensity of 1st peak increased, which implies that dissolved Nb act as another electron transition source.

Keywords *: passivity, semi-conducting property, Photocurrent spectrum, Zirconium alloy, Niobium.*

1. Introduction

Zirconium (Zr) alloys have been used as cladding materials for fuel elements in nuclear reactor system due to their low thermal neutron absorption cross-section, excellent corrosion resistance and good mechanical properties at high temperatures.[1)-3)] Especially, Zr-2.5 wt% Nb alloy is used for pressure tubing for CANDU nuclear reactor because of (i) its better mechanical properties; (ii) improved creep resistance; and (iii) no corrosion rate transition which is observed in the corrosion process of Zircaloys.[1),4)] The excellent corrosion resistance of the alloy in aqueous solution is attributed to the passive film formed on its surface. So the characterization of the passive films is essential to the understanding the corrosion behaviors of these alloys.

Photo-electrochemical method is a very powerful in-situ technique in characterizing the electronic properties of passive films. Application of this method to the analysis of passive films is based on the fact that passive film formed on the surface of metals and its alloys has semi-conducting properties.[2),3),5)-7)] Analysis of passive films by photo-electrochemical method has been mainly focused on thick anodic oxide films grown on pure Zr at anodic potential noble to 3 V_{SCE}.[8)-11)] Only a few papers are concerned with photo-electrochemical analysis of passive films formed at potential lower than 2 V_{SCE} or OCP (open circuit potential).[12),13)] Also there have been few reports of studies describing the effects of alloying elements and 2nd phases on the passive films formed on Zr alloys using photo-electrochemical method. Lee et al [14)] applied this technique to the analysis of passive film of Zircaloy-4, containing Sn, Fe and Cr. And Inagaki et al[15)] reported the effects of alloying elements on oxide films formed under BWR (boiling water reactor) condition by a photo-electrochemical method. However, studies focused on the effects of Nb on the passive films formed on Zr alloys had not yet been reported.

Generally it is agreed that anodic oxide films and passive films on Zr have n-type semi-conducting properties and their band gap energies of 4.5~4.8 eV even though there are some discrepancies depending on electrolytes. Also for the structure of anodic oxides and/or passive films of Zr, many researchers supposed anodic oxide on Zr as a single layer. But Di Quarto et al[13)] suggested duplex structure composed of an outer hydrous oxide layer and an inner anhydrous oxide layer as a structure of anodic oxides and passive films of Zr by using photo-electrochemical method. This was confirmed by Lee et al,[14)] comparing photocurrent spectra of passive films

on Zircaloy-4 with those of thermally grown oxide on the same alloys. Moreover, Patriot et al[16] proved the existence of hydroxide at the outer side of anodic oxide films of Zr using XPS technique.

The research objectives of this study are to investigate the effect of Niobium on the electronic properties of passive films formed on Zr-Nb alloys and to characterize structure and electrochemical behaviors of passive films by comparing photocurrent spectra of passive films with those of thermally grown oxides and oxide formed in water at high temperature and pressure.

2. Experimental

Alloy sheets with various Nb contents of 0, 0.45, 1.5, 2.5 wt% were used in this study. After being held at 105 0℃ for 30 min, specimens were water-quenched and annealed at 750℃, followed by hot rolling and annealing two times, and finally cold rolling and annealing for relieving stress were taken.

A typical three-electrode cell with a quartz window was used for the photocurrent measurement. The working electrodes, Zr-Nb alloys heat-treated as described above, were mounted in epoxy resin and polished with SiC paper to number 2000 grit. Saturated calomel electrode (SCE) and Pt electrode were used respectively as a reference electrode and a counter electrode. All of photocurrent measurements were done in deaerated pH 8.5 borate buffer solution and at room temperature. Before formation of passive film on Zr-Nb alloys, cathodic cleaning at -1.7 V_{SCE} for 10 min. was done to remove air-formed oxide on the metal surface. The 300 W Xenon arc lamp combined with scanning digital monochromator was used to impose a monochromatic illumination to the working electrode. To increase the photon flux, white light from the Xe lamp was focused to the light inlet using two auxiliary focusing lenses.

3. Results and discussion

3.1 Photocurrent spectrum for the passive film formed on Zr-Nb alloy

Fig. 1 shows a potentiodynamic polarization response of Zr-Nb alloys measured at a scan rate at 0.5 mV/s in deaerated pH8.5 buffer solution, where stable passivation occurs over a range of - 0.5 to 1.1 V_{SCE}. Photocurrent spectrum of passive film formed on Zr-1.5Nb at 1 V_{SCE} as a function of incident photon energy ($h\nu$) is presented in Fig. 2. Considering the appearance of anodic photocurrent, it coincided with previous research results, which showed that passive film formed on Zr-Nb alloys has

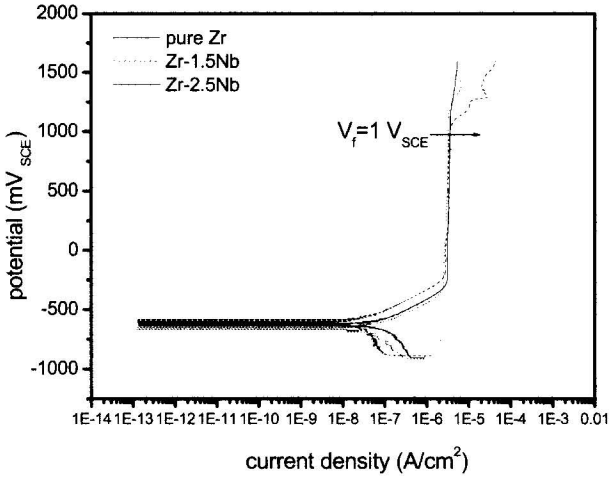

Fig. 1. potentiodynamic polarization responses of Zr-Nb alloys at a scan rate of 0.5 mV/s in deaerated pH 8.5 buffer solution.

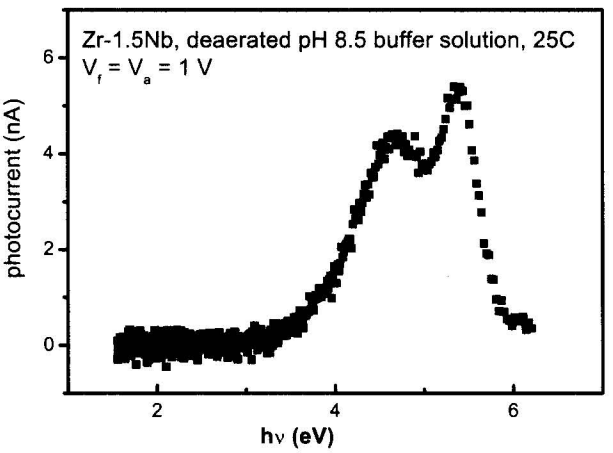

Fig. 2. i_{ph} *vs* $h\nu$ plot for the passive film formed on Zr-1.5Nb alloys at 1 V_{SCE}.

n-type semiconducting properties. Photocurrent began to increase at the incident photon energy of approximately 3.7 eV, exhibited the first photocurrent peak at 4.5 eV, and the second peak at 5.3 eV. Comparing with the photocurrent spectrum of passive film formed on Zircaloy-4 discussed previously,[14] it comes to a conclusion that the passive films formed on Zr-Nb alloy also consisted of duplex layer with an external hydrous layer and an inner anhydrous oxide film, in point that both spectra exhibited two photocurrent peaks at similar incident photon energies. The reduction in the photocurrent intensity after specific photon energy has been attributed to an increase in the surface recombination rate of photo-excited carriers.[17),18)]

3.2 Band-gap energies

The absorption coefficient, α, of crystalline semicon-

ductor is related to incident photon energy by the following equation;

$$\alpha = A(h\nu - E_g)^n / h\nu \quad (1)$$

Where A is a constant, and E_g, the band-gap energy. n depends on the electronic transition types, 1/2 for direct transition and 2 for indirect one. However, 2 is generally accepted to analyze the passive film formed on metals or alloys. The band gap energy for the passive film can be determined from an (i_{ph} $h\nu$) vs. $h\nu$ plot and estimated at the photon energy where i_{ph} is equal to 0, provided that α is proportional to i_{ph}.

Based on the assumption that the Gaussian distribution can be employed to analyze the independent effect of each electron source on the photocurrent spectrum, photocurrent spectrum for the passive film formed on Zr-1.5Nb at 1 V_{SCE} can be resolved into two spectrum components as shown in Fig. 3(a). Fig. 3(b) shows (i_{ph} $h\nu$) vs. $h\nu$ plot of resolved photocurrent spectrum in Fig. 3(a), and band gap energies of each photocurrent spectrum component can be obtained by extrapolation to the incident photon energy axis in (i_{ph} $h\nu$) vs. $h\nu$ plot. From Fig. 3(b), the indirect band gap energy for electron transition, generating photocurrent peak at the incident photon energy of 4.5 eV (named *peak 1* for convenience), was calculated to be 3.31 eV, and the band gap energy for electron transition showing the photocurrent peak at approximately 5.3 eV (named *peak 2*) was to be 4.91 eV. The band gap energies for the passive film form Zr-Nb alloys varying Nb content at the same film formation potential were also obtained in the same way and presented in Fig. 4. Two electron transition are occurred in the passive film formed on Zr-xNb alloys, and band gap energies for each electron transition are approximately 3.01~3.47 eV (E_g^1) and 4.44~4.91 eV (E_g^2). Compared with the indirect band gap energies for the passive film formed on Zircaloy-4,[14] E_g^1, E_g^2 are correspond to the band gap energy of outer hydrous layer and inner anhydrous layer in the passive film formed on Zircaloy-4, respectively. *Thus, peak 1 and peak 2 is presumed to be associated with hydrous ZrO_2, and anhydrous ZrO_2.* With an increase of Nb contents, the band gap energy E_g^1 is slightly increased, but E_g^2 seems to be independent on Nb contents.

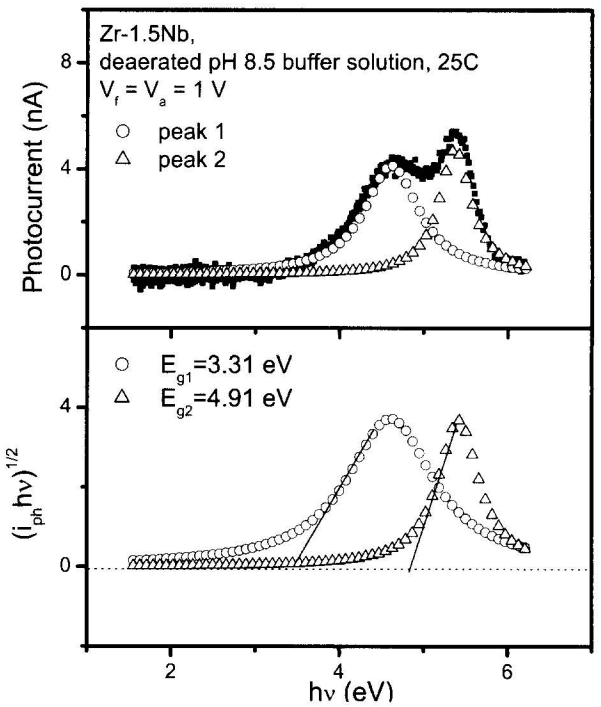

Fig. 3. (a) separation of photocurrent spectra for the passive film formed on Zr-1.5Nb at potential 1 V_{SCE}. (b) determination of an optical band gap energy.

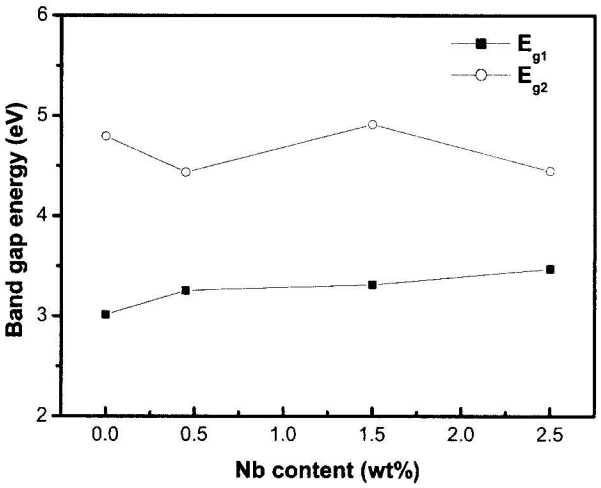

Fig. 4. Effects of Niobium contents on the band gap energy of the passive films formed on Zr-Nb alloys at 1 V_{SCE}.

3.3 Effects of Nb content

Influences of Nb on the photocurrent spectra for the passive film formed on Zr-Nb alloys at 1 V_{SCE} are presented in Fig. 5. Photocurrent began to increase at the incident photon energies of 3.2~3.7 eV, exhibited 1st photocurrent peak (previously named peak 1) at 4.5 eV, and decreased after peak 2 at 5.4 eV. With an increase of Nb content, the relative photocurrent intensity of peak 1 increased even though there was no change in position of incident photon energy at which the photocurrent peak appeared. Fig. 6 shows normalized photocurrent spectra for the passive film formed Zr-Nb alloys with various

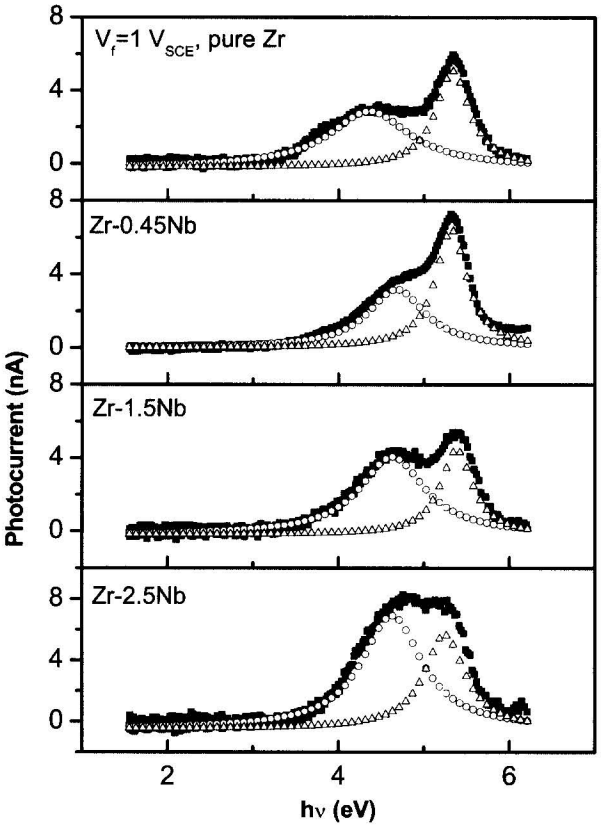

Fig. 5. Photocurrent spectra for the passive films formed on Zr-xNb alloys (x=0, 0.45, 1.5, 2.5) at 1 V_{SCE}.

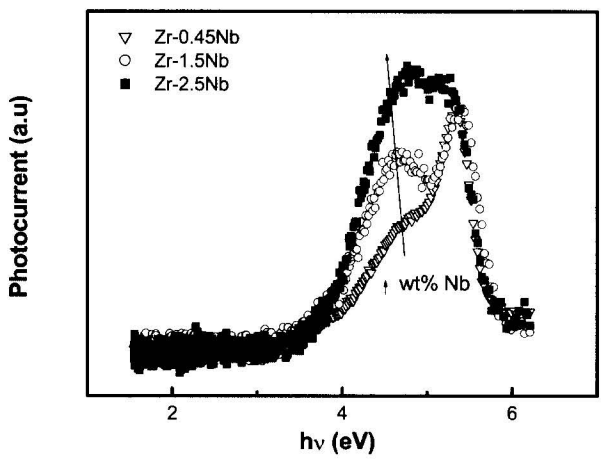

Fig. 6. Normalized photocurrent spectra for the passive film formed on Zr-Nb alloy at 1 V_{SCE} in deaerated pH 8.5 buffer solution at 25℃.

contents of Nb, in which it is clearly observed that the relative photocurrent intensity of peak 1 increases as the Nb content increases.

As mentioned above, from the photo-electrochemical

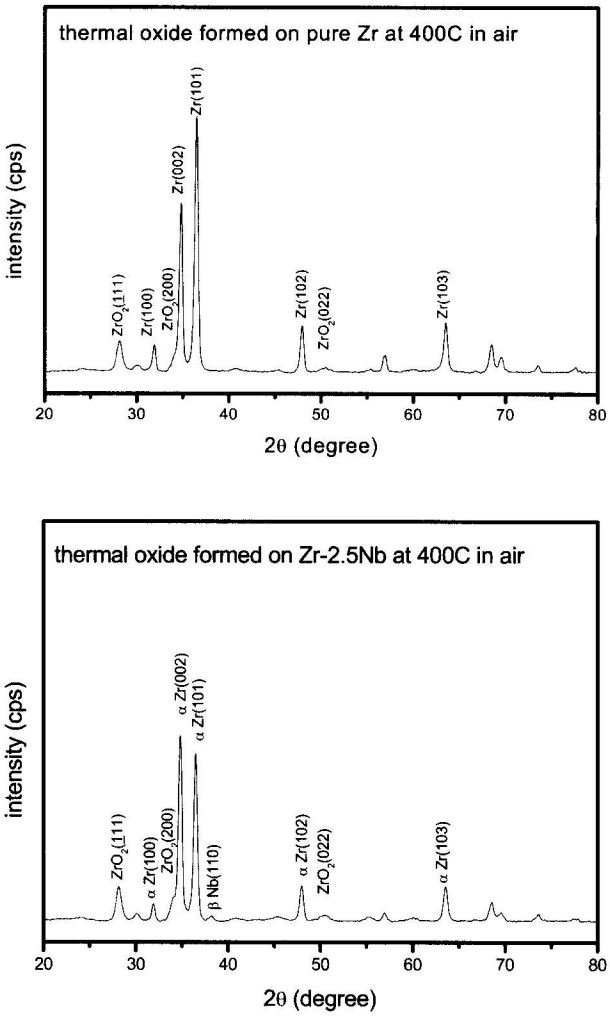

Fig. 7. XRD pattern of thermal oxide grown on (a) pure Zr, (b) Zr-2.5Nb.

studies of passive film formed on Zr and Zircaloy-4, a duplex structure with outer hydrous layer ($ZrO_2 \cdot (H_2O)_n$, $E_g = 2.8 \sim 3$ eV) and inner anhydrous oxide film (ZrO_2, $E_g = 4.5 \sim 4.75$ eV) was suggested.[13,14] This model can be applied to the passive film formed on Zr-Nb alloys. But the effect of Nb on semi-conducting properties of the passive film cannot be explained simply by this model.

In order to examine the effect of Nb on the photocurrent spectra for the passive film formed on Zr-Nb alloys, photo-electrochemical behavior of thermal oxide of Zr-Nb alloy was investigated. Thermally grown ZrO_2, prepared by holding pure Zr and Zr-2.5Nb sample in 400 ℃ air for 1h, have monoclinic crystal structure, confirmed by X-ray diffraction analysis in Fig. 7. Fig. 7(b) shows X-ray diffraction of thermal oxide formed on Zr-2.5Nb, in which the peak at $2\theta = 38.220°$ corresponds to that for β-Nb phase existed in substrate Zr-2.5Nb alloys. So thermal

oxide formed on Zr alloys containing Nb is also confirmed to have monoclinic crystal structure that is same as that of pure Zr. Thermal oxide formed on pure Zr and Zr-2.5Nb alloy were immersed in pH 8.5 buffer solution, and photocurrent spectra were measured by applying open-circuit potential potentiostatically. The measurements were done within 1h after immersion to avoid any structural change of thermal oxide, especially the formation of hydroxide at the surface by adsorption of water molecules. The result is presented in Fig. 8. The overall photocurrent intensities of thermal oxide were significantly decreased compared with those of passive films, which appeared more clearly in the photocurrent spectrum for the thermal oxide formed Zr-2.5Nb alloy. Photocurrent spectrum for the thermal oxide formed on pure Zr in Fig. 8(a) exhibited only one photocurrent peak at the photon energy of 5.7 eV, which seemed to be generated by the same electron transition as that producing the peak 2 in the photocurrent spectrum for the passive film. Thus, the peak 2 in photocurrent for the passive film on Zr alloys appears to be associated with an inner anhydrous ZrO_2 that is similar to the thermal oxide. On the other hand, in the photocurrent spectrum for the thermal oxide formed on Zr-2.5Nb presented in Fig. 8(b), photocurrent began to increase at the incident photon energy of 4 eV, exhibited a shoulder at 4.7 eV, and photocurrent peak appeared at 5.7 eV. This shoulder was observed at the same incident photon energy of the peak 1 in photocurrent for the passive film, however it may not be associated with outer hydrous ZrO_2 because thermal oxide, formed in air, had no hydrous oxide component. Thus, the shoulder expected to be generated by electron transition associated with Nb alloying.

To identify the electron transition source of shoulder appeared at 4.7 eV in photocurrent spectra for thermal oxide formed on Zr-2.5Nb alloy, photocurrent for thermal oxide was measured at corrosion potential after 3 h exposure to the solution at $1V_{SCE}$, presented in Fig. 9. Compared with photocurrent spectrum measured before applying potential, relative photocurrent intensity of shoulder increased. This result demonstrates that a new passive film formed on the pre-existing thermally grown ZrO_2. It was previously reported that by applying potential potentiostatically on thermal oxide immersed into the solution, hydrous oxide formed on the surface of oxide .[14] Thus, an increase of photocurrent intensity of shoulder exhibited at 4.7 eV is considered to be associated with the formation of hydrous ZrO_2. Synthetically photocurrent generated by electron transitions associated with hydrous ZrO_2 and that due to Nb alloying is overlapped in the range of 3.7~5 eV, and appear to have one photocurrent

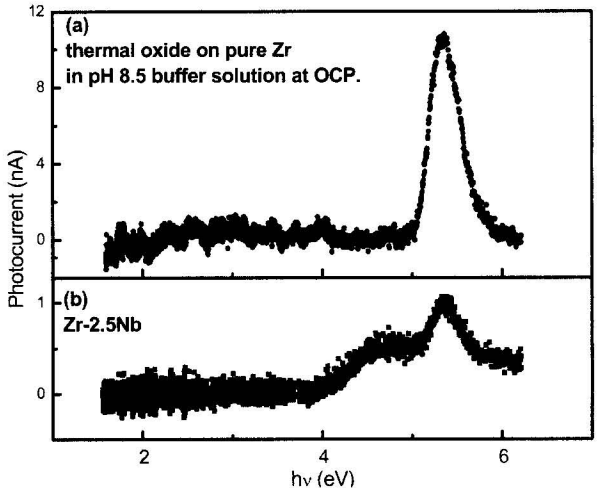

Fig. 8. Photocurrent spectra for ZrO_2 films formed (a) on pure Zr, (b) on Zr-2.5Nb by thermal oxidation at 400°C for 1h in air.

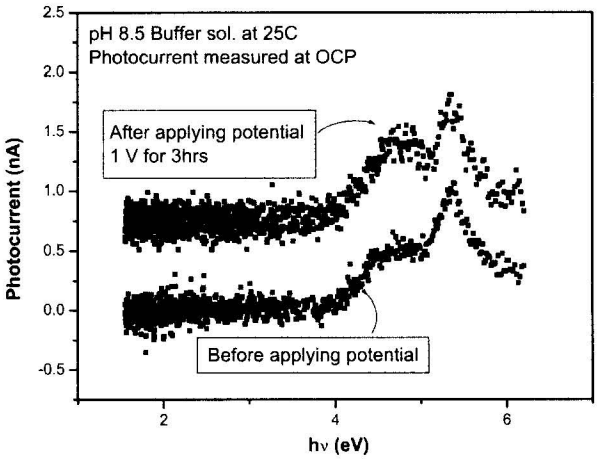

Fig. 9. Photocurrent spectra for thermal oxide formed at 400°C in air. (a) spectrum measured potentiostatically at corrosion potential just after immersion in pH 8.5 buffer solution. (b) spectrum measured at OCP after applying 1V for 3 hours.

shoulder at 4.7 eV. Moreover, this shoulder in the photocurrent spectrum of thermal oxide seems to be generated by the same electron transition source with peak 1 in photocurrent spectrum for passive film.

In conclusion, photocurrent spectrum for the passive film formed on Zr-Nb alloy can be resolved into two photocurrent components, peak 1 and peak 2; peak 1 is generated by overlapping two electron transition, one by external hydrous ZrO_2, the other caused by Nb alloying, whereas peak 2 is associated with anhydrous ZrO_2. The result that Nb acts as electron transition source means alloying Nb affects semi-conducting properties of the passive film formed on Zr alloys.

3.4 Effects of dissolved Nb

Nb alloying into Zr alloy forms new electron transition source, and generates photocurrent peak. To examine the state of Nb causing photo-electrochemical behaviors, heat treatment was taken on the specimen to make Nb dissolved into matrix, and photocurrent measured. The solubility limit of Nb in α-Zr is reported to be 0.5~0.6 wt% even though there are still some discrepancies. Over this solubility limit, the stable structure of Zr-Nb alloys is mixed structure with α-Zr and β-Nb phases. From the X-ray diffraction result(Fig. 7), Zr-2.5Nb specimen used in this study was confirmed to have two-phase structure with α-Zr and β-Nb.

Vacuum sealed Zr-2.5Nb alloy was held at 1050℃ for 20 min. for solution treatment, followed by quenching in water. From the optical microscopic observation after heat treatment, the specimen was consisted of α^{1}- Zr martensitic needles, Nb could not be precipitated as β-Nb, but totally dissolved into matrix by rapid quenching. Photocurrent spectra for the passive film formed on quenched and not quenched specimens at $1V_{SCE}$ are presented in Fig. 10. Compared with photocurrent spectrum for the passive film formed on not quenched specimen, relative intensity of peak 1, partly caused by electron transition created by Nb, was remarkably increased. It suggested that Nb causing electron transition in the passive film is not in the precipitated state, but dissolved state into the matrix.

3.5 Photocurrent spectra for the passive film formed in PWR atmosphere

Zr alloys are mainly used as cladding materials for fuel elements in nuclear reactor system due to their low thermal neutron absorption cross-section, excellent corrosion resistance. Practically cladding tubes are used under PWR (Pressurized Water Reactor) condition.

Fig. 11 shows photocurrent spectrum for passive film formed on Zr alloy under PWR condition. To simulate the atmosphere inside PWR, static autoclave in which temperature was 350℃ and pressure was kept to 16.5 Mpa by adding adequate amount of distilled water was employed. Passive film was formed at open circuit potential on pure Zr and Zr-2.5Nb in this autoclave for 2 h, and photocurrent responses were measured at 1 V_{SCE} after immersion into pH 8.5 buffer solution. For pure Zr, photocurrent began to increase at the incident photon energy of 3 eV, exhibited 1st photocurrent peak at 4.3 eV, and decreased after 2nd peak at 5.5 eV. From an (i_{ph} $h\nu$) vs. $h\nu$ plot, indirect band gap energies were E_g^{peak1}= 2.83 eV, E_g^{peak2} = 4.84 eV each. Compared with the band gap

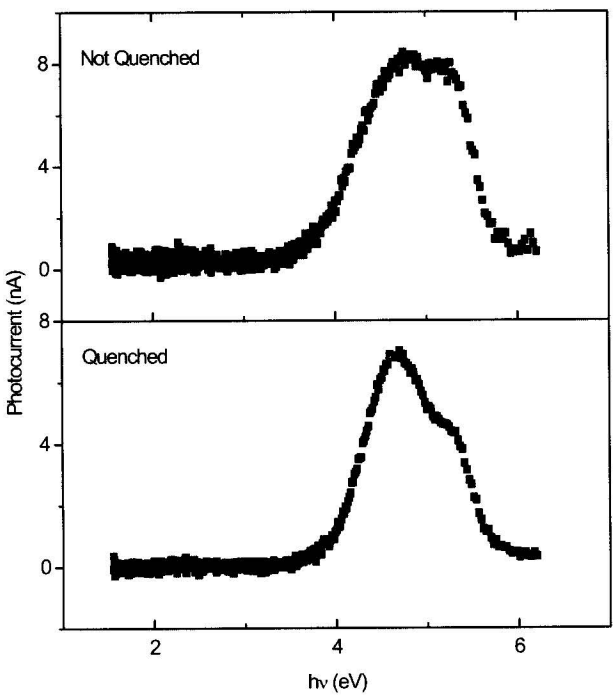

Fig. 10. Photocurrent spectra for the passive film formed on (a) not quenched Zr-2.5Nb alloy (b) β-quenched Zr-2.5Nb alloy.

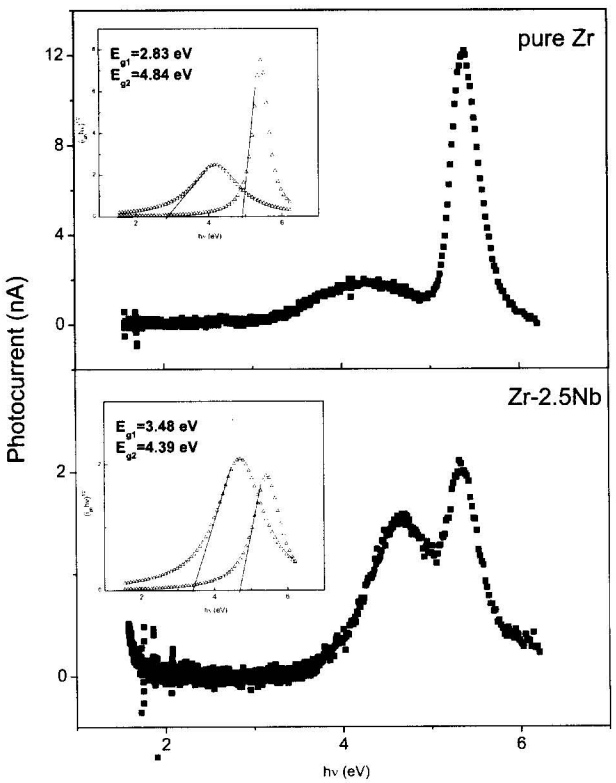

Fig. 11. Photocurrent spectra for the oxide film formed at 350 ℃, 16.5 Mpa (a) on pure Zr. (b) on Zr-2.5Nb alloys.

energies of passive film formed in pH 8.5 buffer solution, 1st peak corresponded to the photocurrent response for hydrous ZrO_2, and 2nd peak for anhydrous ZrO_2.

In contrast, photocurrent spectrum for the passive film formed on Zr-2.5Nb under the same condition is presented in Fig. 11(b). Same with the case of thermal oxide, overall photocurrent intensity was declined. However the relative photocurrent intensity of peak 1 is increased. Indirect band gap energies were E_g^{peak1}= 3.48 eV, E_g^{peak2} = 4.39 eV. From the points that photocurrent intensity of peak 1 relative to peak 2 increased and that band gap energy of peak 1 for the passive film formed at high temperature and high pressure reflected a similar value with that for the passive film formed at room temperature, It seems that electron transition created by Nb also existed in the passive film formed at high temperature and high pressure.

4. Conclusions

1. For Zr-xNb alloys (x=0, 0.45, 1.5, 2.5 wt%), photocurrent began to increase at the incident energy of 3.5~3.7 eV and exhibited the 1st peak (peak 1) at 4.3 eV and the 2nd peak (peak 2) at 5.7 eV. With increasing Nb content, the relative photocurrent intensity of peak 1 significantly increased.

2. Two electron transitions are suggested to explain the photocurrent spectra for the passive film. They appear to originate from an outer hydrous ZrO_2 layer with indirect band gap energy of approximately 3.01~3.47 eV, and from an inner anhydrous ZrO_2 layer with a band gap energy of 4.44~4.91 eV, respectively.

3. Compared with photocurrent spectrum of thermal oxide of Zr-2.5Nb, it was revealed that the photocurrent generated by hydrous oxide and that by another electron transition related to Nb were overlapped one another over the same range of incident photon energy. Thus, the existence of new electron transition occurred by Nb in the passive film formed on Zr-Nb alloy was suggested.

4. In the photocurrent spectrum for passive film formed on Zr-2.5Nb alloy in which Nb is dissolved into matrix as solutes by quenching, the relative photocurrent intensity of 1st peak exhibited at 4.3 eV increased, which implies that the dissolved Nb act as another electron transition source.

5. From the photocurrent spectra for the passive film formed on pure Zr under PWR atmosphere, photocurrent responses for hydrous ZrO_2 and anhydrous ZrO_2 were observed, While that for the passive film formed on Zr-2.5Nb under the same condition, photocurrent peaks due to electron transition created by Nb was exhibited additionally. Thus, it is confirmed that Nb affected electronic properties of passive film formed under PWR condition - high temperature and high pressure water.

References

1. D.G. Franklin and P. M. Lang, in Proc. 9th of Int. Symp. on Zirconium in the Nuclear Industry, ASTM STP 1132, C.M Eucken and A.M. Garde (Eds.), ASTM, Philadelphia, 1991, p3.
2. A. D. Paola, F. Di Quarto, and C. Sunseri, *Corr. Sci.*, **26**, 935 (1986).
3. K. Azumi, T. Ohtsuka, and N. Sato, *J. Electrochem. Soc.*, **133**, 1326 (1986).
4. C. E. Ells, S. B. Dalgaard, W. Evans, and W. R. Thomas, in Proc. 3rd International Conference on Peaceful Uses of Atomic Energy, Vol. 9. p91.
5. T. O. Burleigh and R. M. Latasision, *J. Electrochem. Soc.* **134**, 135 (1987).
6. P. C. Searson, R. M. Latasision, and U. Stimming, *J. Electrochem. Soc.* **135**, 1358 (1988).
7. U. Stimming, *Electrochim. Acta*, **31**, 415 (1986).
8. P. Meisterjahn, H. W. Hoppe, and J. W. Schultze, *J. Electroanal. Chem.*, **217**, 159 (1987).
9. A. Goossens and D. D. Macdonald, *Electrochim. Acta.* **38**, 1965 (1993).
10. A. Goossens, M. Vazquez and D. D. Macdonald, *Electrochim. Acta.* **41**, 47 (1996).
11. S. Preussser, U. Stimming, and K. Wippermann, *Electrochim. Acta.* **39**, 1273 (1994).
12. T. D. Burleigh, Corrosion, **45**, 464 (1989).
13. F. Di Quarto, S. Piazza, C. Sunseri, M. Yand, and S. M. Cai, *Electrochim. Acta.* **41**, 2511 (1996).
14. S. J. Lee, E. A. Cho, S. J. Ahn, and H. S. Kwon, *Electrochim. Acta*, **46**, 2605 (2001).
15. M. Inagaki, M. Kanno, and H. Maki, in Proc. 9th of Int. Symp. On Zirconium in the Nuclear Industry, ASTM STP 1132, C.M Eucken and A.M. Garde (Eds.), ASTM, Philadelphia, 1991, p437.
16. E. M. Patrito and V. A. Macagno, *J. Electroanal. Chem*, **375**, 203 (1994).
17. F. Di Quarto, S. Piazza, and C. Sunseri, in Passivity of metals and semiconductors, Ed. by M. Froment, Elsevier, Amsterdam, 1983, p.497.
18. J. F. MaAleer and L. M. Peter, Faraday Discuss. **70**, 67 (1980).